Macromolecules

Article

Restricted Ion Transport by Plasticizing Side Chains in Polycarbonate-Based Solid Electrolytes

Mahsa Ebadi, Therese Eriksson, Prithwiraj Mandal, Luciano T. Costa, C. Moyses Araujo, Jonas Mindemark, and Daniel Brandell*

Cite This: Macromolecules 2020, 53, 764−774

Read Online

ACCESS | Metrics & More | Article Recommendations | Supporting Information

ABSTRACT: Increasing the ionic conductivity has for decades been an overriding goal in the development of solid polymer electrolytes. According to fundamental theories on ion transport mechanisms in polymers, the ionic conductivity is strongly correlated to free volume and segmental mobility of the polymer for the conventional transport processes. Therefore, incorporating plasticizing side chains onto the main chain of the polymer host often appears as a clear-cut strategy to improve the ionic conductivity of the system through lowering of the glass transition temperature (T_g). This intended correlation between T_g and ionic

conductivity is, however, not consistently observed in practice. The aim of this study is therefore to elucidate this interplay between segmental mobility and polymer structure in polymer electrolyte systems comprising plasticizing side chains. To this end, we utilize the synthetic versatility of the ion-conductive poly(trimethylene carbonate) (PTMC) platform. Two types of host polymers with side chains added to a PTMC backbone are employed, and the resulting electrolytes are investigated together with the side chain-free analogue both by experiment and with molecular dynamics (MD) simulations. The results show that while added side chains do indeed lead to a lower T_g, the total ionic conductivity is highest in the host matrix without side chains. It was seen in the MD simulations that while side chains promote ionic mobility associated with the polymer chain, the more efficient interchain hopping transport mechanism occurs with a higher probability in the system without side chains. This is connected to a significantly higher solvation site diversity for the Li$^+$ ions in the side-chain-free system, providing better conduction paths. These results strongly indicate that the side chains in fact restrict the mobility of the Li$^+$ ions in the polymer hosts.
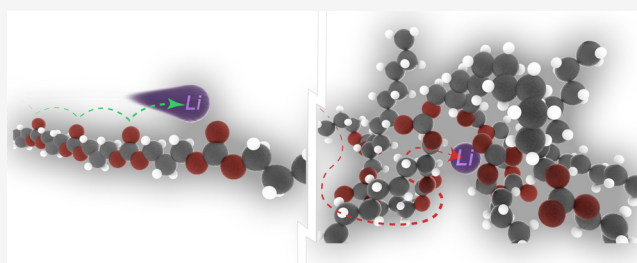
INTRODUCTION

Solid polymer electrolytes (SPEs) are considered as potential candidates in the realization of all-solid-state batteries. SPEs provide higher battery safety by being nonflammable, having sufficient mechanical properties to act as a separator between the electrodes, and having also displayed functionality with the challenging Li metal electrode. However, their lower ionic conductivities as compared to conventional liquid electrolytes remain their largest obstacle.[1]

While there exist several modes of transport for ions in solid polymer materials, two extremes can be distinguished: The first is a strongly coupled motion, where the ions are complexed by the coordinating polymer chains and transported through their segmental motion. New coordination sites appear in the polymer matrix at certain points in time, and the ions are then transported to other coordinating segments by short intra- or interchain jumps. The strong dependence on polymer segmental motion makes the polymer flexibility decisive for ion mobility, and a low T_g, a high degree of free volume, and a large volume of amorphous domains are necessary for fast ion transport.[2,3] Second, a decoupled motion can also be distinguished, where the ions undergo a hopping motion

between fixed sites—again either intra- or interchain—similar to the conduction in a ceramic material.[4] Here, the connectivity of good ionic transport paths is important for ionic mobility, and thereby that the polymer matrix can provide available sites for ions to jump into, while polymer flexibility is less crucial. This renders possibilities to reach "superionic" conductivities, which are not restricted by the Walden rule.[5,6] Naturally, there are also intermediate cases between these two extremes.

The most widely explored polymer hosts for SPEs have been polyethers,[7−9] specifically varieties of poly(ethylene oxide) (PEO) ever since the pioneering studies of Li$^+$ conduction in PEO[10,11] and the application of PEO-based SPEs in Li-metal batteries four decades ago.[12] PEO-based electrolytes are generally semicrystalline materials but with the main conductivity associated with the amorphous phase. This has

prompted the use of strategies to increase the conductivity by decreasing the crystallinity, including plasticizing additives of molecules and particles, and changing the polymer structure through cross-linking and the addition of side chains.[13−15] In addition to acting disruptive to the crystalline structure, flexible side chains may also act plasticizing, increasing the free volume and lowering the T_g.[15−20] Based on a basic understanding of the generally accepted mechanism for ion transport in amorphous and flexible polymer matrices, where the ion movement is coupled to the segmental mobility of the polymer host, this is anticipated to lead to increased ion mobility. The effects of plasticizing side chains are, however, complex. This can be illustrated by the poly(allyl glycidyl ether) system explored by Barteau et al., where the addition of allyl ether side chains to PEO resulted in an increase in ionic conductivity by several orders of magnitude, but *only below the melting point of PEO*, whereas in the amorphous region PEO is still the superior host material in terms of ion mobility.[15] In other systems, oligoether side chains have shown preference for ion complexation and favored ion transport in polycarbonate main-chain systems.[21,22]

Polycarbonate systems such as these have in recent years been highlighted as "alternative" polymer host materials to PEO and other polyethers that have dominated the research field of SPEs.[23] Poly(trimethylene carbonate) (PTMC) has in this context shown promise as an SPE material,[24−27] which can also be modified in a straightforward way by monomer functionalization before ring-opening polymerization, opening up possibilities for synthesizing materials with controlled polymer architectures and tailored functionalities.[28,29] This includes incorporation of plasticizing side chains onto the PTMC backbone.[16,17] Similar to the poly(allyl glycidyl ether) mentioned above, inclusion of side chains in these materials has resulted in significantly lower T_g, but the conductivities of the resulting SPEs did not increase accordingly.[16] This raises questions of whether or not the side chains in fact act to restrict ion mobility in these systems. Such an effect would imply a lack of direct connection between molecular mobility of the polymer host (as determined by the T_g) and the ion mobility.

To probe ion transport in SPEs, molecular dynamics (MD) simulations are the preferred computational methodology due to its ability to study transport properties at an appropriate time and length scale in macromolecular systems.[30] With such approaches, several recent studies have unveiled similar discrepancies between T_g and ion mobility. Instead, the connectivity of solvation sites in the host material has been suggested to be decisive in controlling the movement of ions through the polymer matrix.[31,32] In particular, with interchain transport being decisive for rapid transport of Li+ in SPEs—as recently shown by Brooks et al. for the PEO:LiTFSI system using MD[33]—hindering the transfer of ions between solvation sites will act to severely limit ion transport through the system. This explains why ion transport is much faster in PEO compared to other polyethers with different fractions of ether oxygens in the matrix and thus different solvation site connectivity.[32] Solvation site engineering could also be used as a strategy to raise the cation transference number t_+ by designing polymers with appropriate solvation sites for Li+ cations.[34]

In this current study, MD simulations were used to explore the effect of side chains on the structure−dynamic properties of PTMC-based SPEs and to elucidate the fundamental

mechanisms of ion transport in these systems. To this end, we have synthesized SPE materials with and without side chains (Figure 1), determined their conductivity, and correlated the characteristics of these systems with molecular simulations.
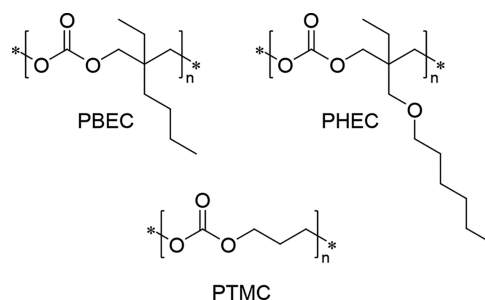

Figure 1. Structures of the three polymers in this study: PTMC, PBEC, and PHEC.

EXPERIMENTAL AND SIMULATION METHODS

Materials and Instrumentation. All chemicals were obtained from commercial sources and used as received unless stated otherwise. LiTFSI (BASF) was dried *in vacuo* at 120 °C for 24 h before use. Trimethylene carbonate (TMC; Richman Chemicals) and all synthesized polymers were stored and handled in an argon-filled glovebox. Poly(2-heptyloxymethyl-2-ethyltrimethylene carbonate) (PHEC) was prepared as described elsewhere.[16] M_n(GPC, THF): 19991 g mol^{-1}, PDI = 1.15.

^{1}H NMR spectra were recorded on a JEOL ECZ 400S 400 MHz NMR spectrometer at 25 °C. The solvent residual peak was used as internal standard. Gel permeation chromatography was performed on an Agilent Technologies 1260 Infinity with PolyPure columns and a refractive index detector. THF was used as eluent at 1 mL min^{-1} at 35 °C. PMMA standards were used for calibration. Glass transition temperatures were determined through differential scanning calorimetry on a TA Instruments Q2000. Two cycles were performed, where samples were cooled to −80 °C at a rate of 5 K min^{-1} and heated to 100 °C at a rate of 10 K min^{-1}.

Synthesis of 2-Butyl-2-ethyltrimethylene Carbonate (BEC) Monomer. In a 500 mL round-bottom flask, 2-butyl-2-ethyl-1,3-propanediol (BEPD) (10 g, 0.062 mol) was dissolved in 100 mL of dry THF. The temperature of the solution was maintained at 0 °C, followed by addition of triethylamine (22 mL, 0.16 mol) under an inert atmosphere. After stirring the mixture for 30 min at this temperature, ethyl chloroformate (15 mL, 0.16 mol) was added dropwise with continuous stirring. The solution was then warmed to room temperature and stirred for 2 h. The precipitated salt was removed by filtration, and the filtrate was concentrated in a rotary evaporator. The product was redissolved in dichloromethane (DCM) and washed with water. The solvent was evaporated, and the crude monomer was distilled under reduced pressure over CaH$_2$ to yield 8 g (73%) of pure product as a colorless liquid (bp 135 °C/1.5 mbar). Material for polymerization was redistilled over CaH$_2$ for sufficient purity. ^{1}H NMR (CDCl$_3$): δ (ppm) = 0.83 (t, 3H, J = 7.3 Hz, −CH$_3$), 0.85 (t, 3H, J = 7.3 Hz, −CH$_3$), 1.11−1.34 (m, 6H, −CH$_2$−), 1.41 (q, 2H, J = 7.7 Hz, −CH$_2$−), 4.06 (s, 4H, −CH$_2$−O). ^{13}C NMR (CDCl$_3$): δ (ppm) = 7.2 (−CH$_3$), 13.8 (−CH$_3$), 23.1 (−CH$_2$−), 23.2 (−CH$_2$−), 24.8 (−CH$_2$−), 29.8 (−CH$_2$−), 33.5 ()C(), 75.2 (−CH$_2$−O), 148.6 ()C=O).

Synthesis of Poly(trimethylene carbonate) (PTMC). 2 g (19.6 mmol) of TMC monomer was combined with 28.8 mg (0.196 mmol of initiator, for DP = 100) of a solution containing benzyl alcohol initiator and 2-(dimethylamino)ethyl benzoate catalyst (1:0.2 molar ratio) in an oven-dried 4 mL vial in an argon-filled glovebox. The mixture was kept with stirring at 50 °C for 46 h for polymerization. The conversion was determined through ^{1}H NMR of samples dissolved in CDCl$_3$ containing 1% benzoic acid to quench the catalyst.

The final product was dissolved in DCM containing a few drops of acetic acid to quench the catalyst before being precipitated in methanol. The resulting polymer was dried under vacuum at ∼37 °C over P_2O_5. Yield: 0.95 g (47%). ^1H NMR (400 MHz, CDCl$_3$): δ (ppm) = 2.07 (m, −CH$_2$−, poly), 4.24 (t, −CH$_2$−O, poly), 5.16 (s, −CH$_2$−O, α-end), 7.33−7.40 (m, −Ph, α-end). M_n (GPC, THF): 6945 g mol^{-1}, PDI = 1.36.

Synthesis of Poly(2-butyl-2-ethyltrimethylene carbonate) (PBEC). 0.931 g (5.00 mmol) of BEC monomer was combined with 100 μL (0.05 mmol of initiator, for DP = 100) of a solution of 0.5 M benzyl alcohol initiator and 0.4 M DBU catalyst in dry toluene in an oven-dried 4 mL vial in an argon-filled glovebox. The vial was kept at 60 °C in the glovebox for 144 h for polymerization. The conversion was determined through ^1H NMR, and the resulting PBEC was purified as described for the synthesis of PTMC. Yield: 0.56 g (59%). ^1H NMR (400 MHz, CDCl$_3$): δ (ppm) = 0.84 (t, −CH$_3$), 0.89 (t, −CH$_3$), 1.15−1.40 (m, −CH$_2$−, poly), 4.00 (t, −CH$_2$−O, poly), 5.15 (s, −CH$_2$−O, α-end), 7.36−7.40 (m, −Ph, α-end). M_n(GPC, THF): 14384 g mol^{-1}, PDI = 1.27.

Polymer Electrolyte Preparation and Characterization. PTMC, PBEC, or PHEC together with LiTFSI were dissolved in THF. The Li$^+$ to carbonyl oxygen ratio was kept at 0.08 for all samples. The solutions were poured into Teflon molds or glass vials before they were put in a vacuum oven at 40 °C for 20 h at 200 mbar, followed by 60 °C for 40 h at 2 mbar. The polymer electrolytes were then placed between two stainless steel blocking electrodes in a Swagelok cell. The thickness was controlled by a Teflon film spacer. Electrochemical impedance spectroscopy measurements were conducted with a Schlumberger SI 1260 over a frequency range of 1 Hz− 10 MHz and an amplitude of 10 or 35 mV from room temperature up to around 90 °C. The data were fitted to a Debye equivalent circuit, and the total ionic conductivity was calculated from the bulk resistance. The ionic mobility of Li$^+$ was also calculated from the ionic conductivity based on the Nernst−Einstein equation and the Einstein relation. The density used to calculate the ion concentration was determined by weighing a known volume of sample (∼50−200 μL, calibrated exactly with water).

Molecular Dynamics (MD) Simulations. MD simulations were performed by using the Gromacs suite package, version 2018.[35,36] Polymer electrolyte simulation boxes were constructed by considering 32 chains of polymer, 46 TFSI anions, and 46 Li$^+$ ions ([Li$^+$]: [carbonate] = 0.08). Each chain of polymer had 18 repeating units, and to avoid end-group effects in the relatively short chains, the potentially ion-coordinating hydroxyl end-group present in each of the synthesized polymers was replaced with a noninteracting benzyl group at the ω-end. The packing of the particles in the simulation boxes was built by using the Packmol package.[37] OPLS-AA force fields[38] were applied to describe the interactions within the simulated systems for the polymer chain and the Li ion. The force field parameters for the TFSI ion were adopted from Padua and Lopes.[39] All force field parameters for the polymer chains were adopted from the OPLS-2005 Maestro package to construct the initial topology for the polymer chains,[40] after which the Intermole software[41] was used to convert the topology format.

Because the electrostatic forces are highly influential for the description of transport properties in polymer electrolyte systems, the Chelpg scheme[42] in the Gaussian 2016 package[43] was used to calculate the charges for trimers of each of the repeating units in the study. The B3LYP hybrid functional[44,45] with a aug-cc-pvdz basis set[46] was applied for these calculations. These were used to specifically refine the charges of the atoms in the functional parts of the polymer; i.e., O and C of the carbonyl unit, the "ethereal" O of the carbonate unit and in the side chain in PHEC, and the carbon atoms connected to the side chain oxygen. An average of the charges calculated by this scheme replaced the charges assigned from the OPLS force field while keeping the charge neutrality of the polymer chains. The resulting partial charges used are reported in Table S1. A scaled charge model was considered by setting the Li$^+$ and TFSI ions to +0.8e and −0.8e, respectively, and used for all data presented apart

from Figure S4. The same charge scaling was used in a previous MD study of polymer−ionic liquid systems.[47]

Periodic boundary conditions were applied in the MD simulations. The energy minimization procedure was performed by a steepest descent algorithm. A leapfrog integrator was applied for the integration of the equation of motion with a time step of 1 fs. To achieve accurate densities of the polymer electrolytes after equilibration in the NVT ensemble, equilibrations were performed in the NPT ensemble by using a Berendsen barostat with a coupling time of 1.0 ps at 500 K. The output after this procedure were then used for simulation at 300 K for 50 ns. Temperatures of 423, 380, 348, 320, 280, and 260 K have thereafter been considered. For each temperature, the initial structures were taken from the equilibrated 300 K system and 50 ns NPT equilibration was applied for all simulations at the desired temperature until a reasonable average density was achieved. Finally, production runs for 200 ns were performed for each temperature by using a Parrinello−Rahman barostat and a coupling time of 5.0 ps. To calculate the glass transition temperature (T_g) of the polymer electrolytes, separate simulations were conducted by using an annealing process where the electrolytes were cooled from 423 to 163 K by 10 K increments. At each temperature, a NPT equilibration for 5 ns was performed while the cooling process to the lower temperature was also set to 5 ns. Finally, the average density after the 5 ns NPT equilibration at each temperature was used to plot the density vs temperature to estimate the T_g values. For some of the postprocessing analysis, the MD simulations were continued to longer time (1 μs) to obtain a wider relaxation window for the dynamics properties.

■ RESULTS AND DISCUSSION

The versatility of the six-membered cyclic carbonate monomer platform enables facile preparation of polymers where the ion-coordinating carbonate ester groups are complemented by specific functional groups. Here, we turn our interest toward materials with plasticizing side groups and have considered three carbonate-based host polymers: PTMC, PBEC, and PHEC (Figure 1). While PTMC has a backbone without side chains, PBEC contains relatively short noncoordinating side chains, and PHEC is characterized by a longer side chain that also includes a potentially ion-coordinating ether oxygen. The polymers were synthesized through ring-opening polymerization of the respective cyclic monomers, aiming for a degree of polymerization (DP) of 100 for all materials to ensure that the chains are sufficiently long for ion transport to take place solely through segmental motion rather than vehicular transport, enabling direct correlation with high-molecular-weight systems. The molecular weight and polydispersity index for the three polymers, as obtained from GPC, are reported in Table 1 along with their density. Electrolytes were prepared by combining the polymers with LiTFSI salt through solvent casting. The salt concentration was kept relatively low at 12.5

Table 1. Glass Transition Temperatures (T_g) from DSC Measurements and from MD Simulations for the Three SPEs (Concentrations of [Li$^+$]:[Carbonate] = 0.08)^a

| polymer host | T_g (°C) | | M_n (g mol^{-1}) | PDI | density (g cm^{-3}) |
	simulation	experiment			
PTMC	0	−9.6	6945	1.36	1.2
PBEC	−10.5	−14	14384	1.27	1.0
PHEC	−31.3	−45	19991	1.15	1.1

^{a}Molecular weight (M_n) and polydispersity index (PDI) for the three polymers were obtained from GPC. Densities were obtained by weighing a known volume.

carbonyl oxygens per Li$^+$ ([Li$^+$]:[carbonate] = 0.08) to promote Li$^+$ solvation and ion separation to avoid significant ion−ion interactions and clustering, as ion aggregation may result in alternative transport mechanisms that are beyond the scope of this study.[48,49] Interestingly, the addition of salt did not change the density to a measurable degree, which indicates that it is the weaker intermolecular interactions due to the dilution of the carbonate groups in the side-chain systems which is the main cause for the differences among the systems.

The plasticizing effects of the side chains are obvious from the measured T_g values for the different polymers (Table 1). The DSC scans are also shown in Figure S1. As expected from the structures, the PTMC-based SPE has the highest T_g of the three systems at −9.6 °C, while the longer side chain in PHEC decreases the T_g of the resulting SPE significantly to −45 °C. The T_g of the PBEC electrolyte is found at an intermediate level: −14 °C. The T_g values were also estimated from the MD model. The plots of calculated density from the MD simulations with respect to the various temperature and the intersection of the higher and lower regions (the selected points for T_g estimations) are shown in Figure S1. As can be seen in Table 1, the trend and the values seen in the experimental results were largely reproduced by the MD model (within 10% for the density values). The somewhat higher T_g values obtained from the MD simulations are expected due to the slower cooling and higher molecular weight applied experimentally, which is impossible to reproduce in simulations.[31,50]

The total ionic conductivities measured experimentally for the three polymer electrolytes are presented in Figure 2. On the basis of the T_g values and considering coupling to
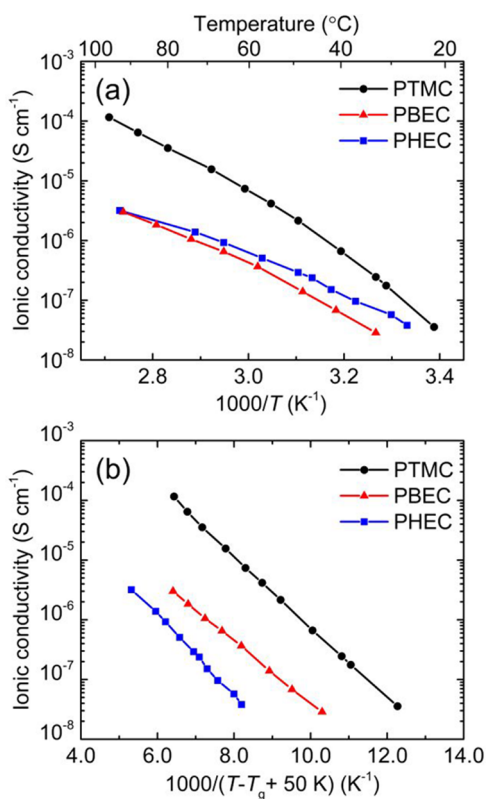
segmental motions as the main ion transport mechanism, it can be expected that the trend in ionic conductivity would follow the inverse trend of the T_g. On the contrary, we instead observe that the PTMC electrolyte displays the highest conductivity throughout the measured temperature range. Following the approach by Pesko et al.,[51] the effects of the side chains were evaluated independently from the effects of differences in T_g by plotting the ionic conductivities on a shifted temperature scale of $1000/(T - T_g + 50 \text{ K})$ (Figure 2b). Through this transformation of the data, the influence of the segmental mobility of the host polymer on the ionic conduction is corrected for while instead the influence of structural features are emphasized. This highlights the intrinsic conductivity originating from the polymer's structure, rather than its general flexibility. As seen in Figure 2b, the differences between the electrolytes are now much more obvious, and the trend in conductivity follows the order PTMC > PBEC > PHEC; i.e., when considering the ion transport independently of the molecular mobility of the polymer host, the ionic mobility is clearly negatively influenced by the presence of side chains on the polymer backbone. It is also clear that PHEC, which has longer side chains than PBEC, has the lowest conductivity when its much lower T_g is accounted for. The same trend can be seen when plotting the data in terms of ionic mobility, presented in Figure S2, which corrects for the differences in molar concentrations of the species. This indicates that the side chains in both PBEC and PHEC, although rendering a much lower T_g, also induce restrictions in the mobility of ions between the coordination sites in the polymer matrix.

The ionic conductivities were also calculated from the MD simulations based on the Nernst−Einstein (NE) equation (assuming unrelated diffusivity of the ionic species; see details in the Supporting Information), and the results are presented in Figure S2 and Table S2. The mean-square-displacement (MSD) function of the center of mass of Li$^+$ and TFSI ions for 1 μs simulations was used to estimate their respective diffusion coefficients (see Figure S3 and Table S3). Generally, three different regimes can be observed in the log−log scale MSD plots: ballistic-like motions ($\langle\Delta r_i(t)^2\rangle \propto t^2$) at short time scales; a subdiffusive regime ($\langle\Delta r(t)^2\rangle \propto t^x$ with $x < 1$) where the MSD is more flat and the particle motions are restricted by the surrounding atoms; and a third regime with closer to a linear relationship, approaching the diffusive regime ($\langle\Delta r_i(t)^2\rangle \propto t$). For longer simulation times, up to 1 μs, the slopes of the MSD plots are still less than unity, indicating that the ionic mobility is still not completely diffusive. This is not unexpected; reaching a fully diffusive regime in MD simulations of SPE systems has previously been reported to take very long simulation times at these temperatures.[31] Because of noisy data appearing at the end of the simulations (the last 200−300 ns) for some systems, the linear fitting and calculation of the diffusion coefficients were performed in the range 400−500 ns for all temperatures (see Table S4 for the corresponding calculated slopes of log−log plots).

It can be seen in Table S2 that the general trend of ionic conductivities from simulations is in good agreement with the experimental results and that PTMC exhibits higher ionic conductivity than PBEC and PHEC. This trend is especially clear at higher temperatures.

The MSD plots for all different species at different temperatures in Figure S3 show, as expected, that the ionic displacement increases with increasing temperature in all three

Figure 2. Total ionic conductivity of PTMC, PBEC, and PHEC obtained experimentally and plotted versus (a) $1000/T$ and (b) $1000/(T - T_g + 50 \text{ K})$.

SPEs. The MSD plots calculated at 423 K for Li$^+$ and TFSI ions are also presented in Figure 3. Figure 3a shows that the
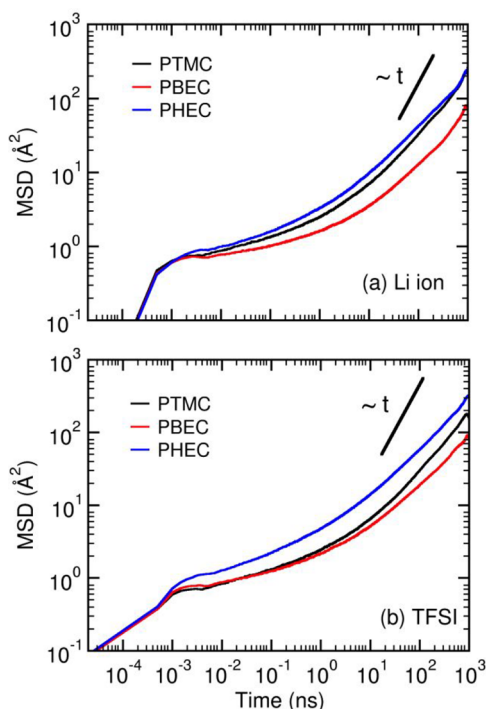

Figure 3. MSD for the center of mass of Li$^+$ and TFSI in PTMC, PBEC, and PHEC electrolytes at 423 K obtained by using the scaled-charge model. The short black line ($\sim t$) is added for visual aid to show the slope = 1 in the log−log plot.

Li$^+$ ion diffusivity is less restricted by the surrounding atoms (polymer and anion) in PHEC and PTMC than in PBEC, since the intermediate regime is shorter in the former cases than in the latter. Similarly, the intermediate region of the MSD plot for TFSI is shorter for PHEC than for PTMC and PBEC. The overall observation from both anion and cation MSD plots is that both ionic species are less restricted by the surrounding atoms in PHEC, which also has the lowest T_g. The longer intermediate region for the Li$^+$ ion in PBEC could be due to a hindering effect of the side chains, i.e., a type of caging effect. However, the effect of the side-chain polymer architecture on the ionic diffusivity is far from clear from the MSD results of either of the studied SPEs.

To elucidate the effects of the side chains on ion movement in the different polymer matrices, the coordination structures as obtained from the MD simulations can provide useful insights. The coordination environment of the Li$^+$ ions in the SPEs has a significant effect on the ion dynamics since the coordination shells are the solvation sites for the ions in the polymer hosts. A few random snapshots of the Li$^+$ ion coordination shells from the MD simulations performed at 423 K are presented in Figure 4, together with radial distribution functions (RDFs; $g(r)$) and the cumulative coordination numbers (CN, $n(r)$) for Li$^+$−O$_{polymer}$ and Li$^+$−O$_{TFSI}$ from scaled-charge MD simulations at 423 K (results from non-scaled-charge models are shown in Figure S4). There are large similarities in the RDFs obtained at other temperatures, meaning that these structures are largely temperature-independent.

It can be seen from Figure 4 that the main-chain carbonyl oxygen and TFSI oxygen atoms are surrounding the Li$^+$ ion in the first coordination shell in all three SPE systems. For PTMC, the average number of carbonyl oxygens and TFSI surrounding the Li$^+$ ion in the first coordination shell (0.2 nm) is around 3 (CN(Li−O$_{carbonyl}$) = 2.8) and 1−2, respectively. This is in agreement with previously reported results from MD simulations and NMR studies.[52] The ethereal oxygens of PTMC are found in the second coordination shell (0.4 nm) around the Li$^+$ ion with an average number of 6, directly corresponding to the number of surrounding carbonate groups, indicating that these are not directly involved in coordinating the Li$^+$ ions. In PBEC, the first coordination shell around the Li$^+$ ions consists of oxygen atoms of TFSI and carbonyl oxygens of the polymer (CN(Li−O$_{carbonyl}$) = 2), at the same distance as in PTMC, but with an increased degree of ion pairing as seen from the higher CN for TFSI. This corresponds to a poorer solvating effect of the polymer as compared to PTMC and is consistent with the increased nonpolar character of the polymer with the addition of the alkyl side chains. The same trend can be observed in the second coordination shell of Li$^+$ ions in PBEC, which also displayed higher CNs for TFSI oxygens and lower for ethereal oxygens in the polymer. In PHEC, on the other hand, the observed pattern in the first coordination shell (0.2 nm) is more or less similar to PTMC (CN(Li−O$_{carbonyl}$) = 2.5). Moreover, it can be seen in Figure 4c that the side-chain ether oxygen in PHEC is not directly involved Li$^+$ ion coordination. This is consistent with earlier studies that report preferential coordination to main-chain carbonate groups over single ether groups both in side chains[17] and in the main chain.[53] Among the polymers, PBEC clearly stands out with much lower ion−polymer interactions. This is also complemented with a higher degree of ion paring between Li$^+$ and TFSI. Thereby, a hindering effect of the side chains seems to exist, which reduces the interactions of the Li$^+$ ions and the carbonyl oxygen of the backbone of the polymer.

The number of polymer chains involved in the first coordination shell of the Li$^+$ ions was also analyzed for all Li-ion trajectories. The average number of polymer chains coordinating to Li$^+$ ions is 2.84, 2.19, and 1.65 for PTMC, PBEC, and PHEC, respectively. Considering that the Li$^+$−O$_{carbonyl}$ CN is not strikingly different for the three different polymer hosts, this is equivalent to a significantly higher amount of interchain coordination for PTMC vs intrachain coordination for PHEC. Because the binding motifs are identical in all three polymer hosts, these differences cannot be explained by chelating effects. Instead, this indicates that the PTMC chains can more easily come into close proximity of each other compared to the other host materials. With the chains of the host polymer closer together, the side-chain-free PTMC system should more easily be able to form potential solvation sites and should thus have a higher connectivity between these solvation sites.

For comparison, RDFs and coordination number were also calculated by the non-scaled-charge model (see Figure S4). Although these results display more or less the same trend as in the scaled-charge model (Figure 4), it can be clearly seen that the CN to anion oxygens increases without charge scaling in all three SPEs. This is natural since the charge scaling decreases the Coulombic interactions and thereby renders ion−ion attractions less strong, thereby resulting in a lower ionic aggregation. The application of scaled-charge models is supported in polymer electrolyte systems since it has been
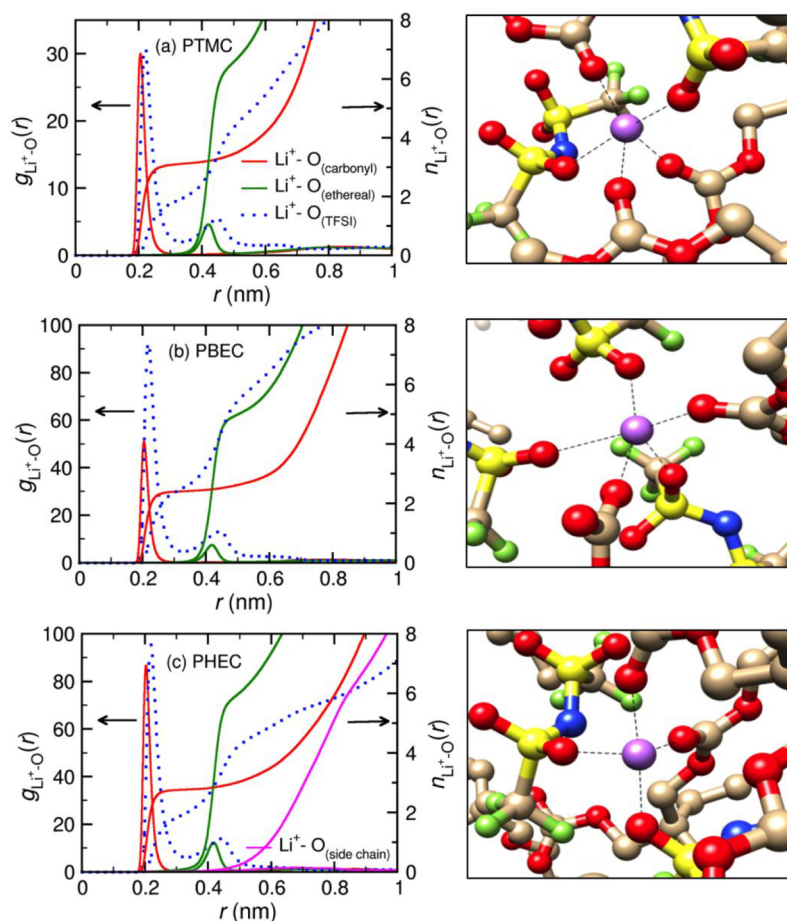
Figure 4. Snapshots of Li$^+$ ions with the surrounding polymer and TFSI ions within 2.5 Å observed in the MD simulations and radial distribution functions (the left y-axis), $g(r)$, with average coordination number (the right y-axis), $n(r)$, for Li$^+$–O in (a) PTMC, (b) PBEC, and (c) PHEC electrolytes, at 423 K. Red, light brown, green, blue, yellow, and purple denote O, C, F, N, S, and Li, respectively.

found to be essential to reproduce several structural and transport properties.[47,54]

To further investigate the dynamics of the Li ions in the three polymer electrolytes, the contact autocorrelation function (ACF) of polymer–Li$^+$ and TFSI–Li$^+$ have been calculated (see the Supporting Information). The autocorrelation function $C(t)$ depends on pair formation within a predefined cutoff distance and decreases sharply to lower values if the contact time between the selected particles is short. Here, the contact distances for Li$^+$ with carbonyl oxygen (Figure 5a) and TFSI oxygen (Figure 5b) are considered within 2.5 Å and displayed for 423 K. The decays of $C(t)$ for SPEs are generally quite slow; for example, extending the simulations from 500 ns to 1 μs was necessary to properly reduce the $C(t)$ values in the tail of the plot.

The MSDs of the carbonyl oxygen for the three polymers are also calculated at 423 K and shown in Figure 5c to better observe the correlation of Li$^+$ ion mobility and the diffusion of O$_{carbonyl}$. Furthermore, the log–log scale MSDs of both carbonyl and ethereal oxygens in the polymers at all temperatures are plotted in Figure S5. The higher MSD of O$_{carbonyl}$ in PHEC is correlated to a seemingly higher mobility of Li$^+$ ions (seen in Figure 3a), which could well be a result of higher Li$^+$ diffusivity as compared to PBEC. For PTMC, on the other hand, the MSD of the carbonyl oxygen is lower than in PHEC, while the estimated Li$^+$ diffusion coefficient at this temperature is actually slightly higher in PTMC than in PHEC

(see Table S3). Together with the ACF plots (Figure 5a,b), this suggests that the Li$^+$ mobility in the side-chain-containing PBEC and PHEC is more correlated to coupled ion–polymer motion (via interactions with carbonyl oxygens) than to changes in the coordination environment (solvation sites), while local changes in the structural environment constitute an active transport mechanism in PTMC.

The MSDs of Li$^+$, TFSI, and the polymer carbonyl oxygens are presented in Figure S6. As expected, the polymer atoms are the most mobile species in all investigated systems, while—as discussed above—the diffusivity seems generally higher in the PHEC system. This corroborates the impression that while the general dynamics are correlated to the low T_g (as for PHEC), this is not necessarily connected to the ionic transport. It is also interesting to note that although the MSDs are very similar for the ionic species (especially for PTMC and PBEC), the correlation of their motion is not highly significant (Figure 5b).

To gain insight into the kinetics of these processes, the residence time (or lifetime), τ_{res}, of the Li$^+$ ions in the respective coordination environments can be obtained from the ACF plots through several methods;[55,56] here, the best fit was obtained by a summation of multiple exponential functions and subsequent integration (see the Supporting Information for the mathematical description used).[57] The obtained τ_{res} values at 423 K are reported in Table 2. It can be seen clearly in Figure 5 that the $C(t)$ of PTMC decays sharply to lower
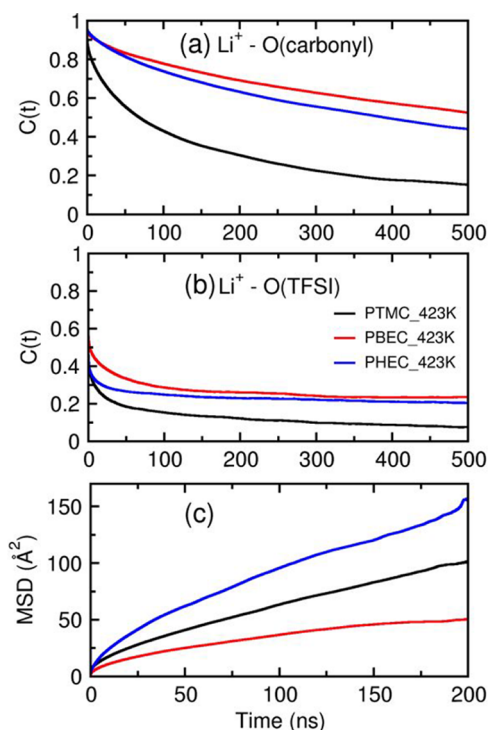
Figure 5. Contact correlation functions of Li$^+$ and (a) carbonyl oxygen of the polymers and (b) TFSI oxygens. (c) MSD of carbonyl oxygen of the different polymer chains at 423 K. Note the different time scale in (c).

Table 2. Residence Time τ of Li$^+$–O$_{carbonyl}$ and Li$^+$–O$_{TFSI}$

polymer host	$\tau_{\text{Li}-\text{O(carbonyl)}}$ (ns)	$\tau_{\text{Li}-\text{O(TFSI)}}$ (ns)
PTMC	157	62
PBEC	338	134
PHEC	309	116

values, in stark contrast to PBEC and PHEC. This is reflected in the residence times, confirming that the duration for Li$^+$ ions around both coordinating carbonyl groups and anions is significantly shorter in PTMC than in both PBEC and PHEC, thus indicating a much more rapidly changing coordination sphere. The difference between the Li$^+$ residence times in PBEC and PHEC is insignificant as compared to the residence time in PTMC, thus showing that the side chains are highly influential on the possibility to interchange the coordination sites around Li$^+$.

Another important observation is the contact of Li$^+$ with the anions. Although the ion–polymer interactions are considered the most decisive factor for conductivity in classical SPE theory, the anions are also highly influential on the movements and diffusion of Li$^+$ in the electrolyte, and we can observe extensive ion pairing also at this low salt concentration. Therefore, the longer duration of the Li$^+$–O$_{TFSI}$ contacts in PHEC and PBEC is likely having an effect on the overall mobility of Li$^+$ ions in these systems. This can also be an indication of higher ion clustering in PBEC and PHEC than in PTMC, which is also seen from higher CNs in the RDF plots (Figure 4). This appears to be well-correlated to the residence time (Table 2), where the ion pairing forms more stable solvation sites and thereby more fixed Li$^+$ ions.

While the data discussed so far have been based on average values over time and/or over the entire ensemble of polymer

chains, a full description of the ion transport mechanism requires a detailed look at individual ion movements. To investigate the nature of the polymer solvation sites and the possible ion transport mechanisms in these polymer hosts, the changing coordination environment of the Li cations during a simulation time of 200 ns was therefore studied by monitoring the indices of coordinating carbonyl oxygens (within 2.5 Å)— i.e., where the different coordinating carbonyl oxygens had unique identities and were not the same throughout the simulation—for randomly selected Li$^+$ ions in the polymer electrolytes. The procedure follows similar methods applied for PEO-based SPEs.[31,33] Representative time evolution plots are presented for individual Li$^+$ ions in Figure 6a−c for the three different polymer hosts, where also interchain and intrachain coordination environments are visible through the horizontal gray lines in the plots. Here, the blue dots represent individual coordinating carbonyl oxygens around a specific Li$^+$. A change in the indices for the coordinating oxygens (as in Figure 6a) means that there is an interchange of carbonyl groups and thus a novel coordinating environment for the Li$^+$ under study.

In Figure 6a, interchain hopping can be seen occurring at several points throughout the simulation. Intrachain hopping, on the other hand, is a comparatively less frequent event, which correlates well with previous work on ester-based SPEs where moving ions primarily are characterized by interchain mobility.[31] In PBEC (Figure 6b), the lines are considerably more static, indicating that neither intrachain nor interchain hopping is significant. Therefore, in PBEC, the segmental motion of the polymer chain itself is the main reason for the observed ionic mobility. Also Figure 6c, representing a Li$^+$ in PHEC, is more static compared to PTMC. Because the coordination sphere for these cations is more or less fixed throughout the simulation, the observed ionic mobility here does not represent any true transport in a macromolecular system, where a changing coordination sphere would be necessary due to the insignificant mobility of the polymeric solvent at the macroscopic level.

To better quantify the examples shown in the time evolution plots (Figure 6a−c), the first coordination shell for all Li$^+$ ions in every MD box was analyzed in every frame within a 200 ns trajectory. The numbers of unique solvation sites based on the 2.5 Å distance criterion were counted, and the results are presented in Figure 6d. It should be mentioned that the numbers in Figure 6d are the different solvation sites (considering the combination of index numbers of the carbonyl oxygens) observed during the simulation time and not their frequency of occurrence. Moreover, while these coordination environments generally have certain carbonyl oxygens in common, they represent unique combinations of different carbonyl groups, i.e., different solvation sites.

From these data, we clearly see that the Li$^+$ ions in PTMC pass through many different solvation sites throughout the simulation, which is indicative of a rapidly interchanging coordination environment. This is also reflected in the τ_{res} already discussed and serves well to explain the much higher conductivity compared to the other systems. The side-chain-incorporating PBEC and PHEC systems, in turn, show comparatively few interchanges of coordination sites despite the lower T_g, which indicates that there is indeed a restrictive effect of the side chains. This clearly confirms that Li$^+$ ions move more freely to different solvation sites in PTMC than in PBEC and PHEC and is well-correlated to the experimentally observed ionic conductivity.
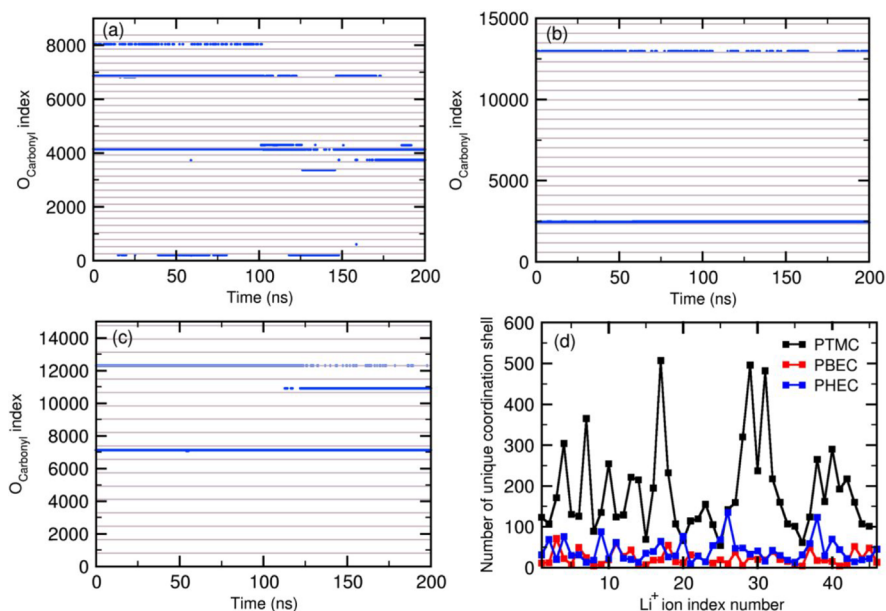
Figure 6. Examples of the time evolution of Li$^+$ coordination environments for (a) PTMC, (b) PBEC, and (c) PHEC at 423 K. The y-axis represents the index numbers for all different carbonyl oxygens in the MD simulation boxes. Changing (blue) lines represent a changing coordination sphere around Li$^+$, while straight blue lines represent a fixed Li$^+$–O$_{carbonyl}$ coordination throughout the simulation. Moreover, a polymer chain is confined between two horizontal gray lines. If several (blue) coordination lines are within the same gray lines, this represents intrachain coordination. (d) Number of unique coordination environments around Li$^+$ throughout 200 ns trajectories in PTMC, PBEC, and PHEC for all Li$^+$ in the simulation boxes at 423 K.

These fundamental aspects of how the structure of the polymer and the local coordination around Li$^+$ control the possibility for ionic transport in these systems are illustrated in Figure 7, where a few selected time frames for the Li$^+$ ions considered in Figure 6a−c are illustrated. For PTMC (Figure 7a), a typical interchange of ligand carbonyls around the Li$^+$ ion can be observed, i.e., a change of the solvation site. At 125 ns, the Li$^+$ ion has three different carbonyl O atoms in the first coordination sphere (within 2.5 Å). In the next frame shown (125.3 ns), a new carbonyl group has moved into the coordination sphere, followed by yet another carbonyl group at 126.1 ns. Simultaneously, one of the originally coordinating carbonyl oxygens leaves the coordination sphere, rendering a novel solvation site for Li$^+$ at 137 ns. During this sequence, the Li$^+$ ion has moved relative to the polymer host. Considering the relatively high frequency of these events for PTMC (seen in Figure 6d), PTMC seems to provide a good solvation site connectivity. This type of Li$^+$ ion mobility is similar to the mechanism defined as a "shift" by Brooks et al.[33] for SPE systems.

In contrast to PTMC, PBEC (Figure 7b) and PHEC (Figure 7c) display a hindering effect of the side chains, as illustrated in two time frames for each system (125 and 140 ns). Here, the side chains effectively restrict the possibility for the carbonyl groups of adjacent chains to move closer to the cation, thereby not providing the sought connectivity between different solvation sites.

■ CONCLUSIONS

The strategy of incorporating flexible side chains in polymer electrolytes to improve the ion dynamics is at best a double-edged sword; while the segmental mobility of the polymer host can indeed be drastically increased, a corresponding increase in conductivity is not observed. We have here investigated the structure–dynamic properties of SPEs comprising the polycarbonate host materials PTMC, PBEC, and PHEC by a combination of MD simulations and experimental measurements. PBEC and PHEC have a lower T_g than PTMC due to the side chains in their structures. Although this can be expected to result in higher ionic conductivities, the reverse phenomenon is observed: PTMC displays the highest conductivity. The MD simulations here help to explain this relationship.

Through the MD simulations, the residence time is found to be comparatively much shorter for the coordinating carbonyl groups in PTMC, which is also reflected in a rapidly changing coordinating environment. Primarily, the ions are transported through interchain hopping in PTMC, and the polymer structure clearly promotes interchain coordination. The side chains of PBEC and PHEC instead restrict the possibilities for changing the coordination sites, leading to less interchain coordination and what appears to be a break in the connectivity between possible coordinating environments in the polymer matrix. This would explain the more rapid changes in ionic coordination for Li$^+$ in PTMC. In contrast, for the systems with side chains, the ions are instead relatively stationary but display mobility through a correlated movement with the macromolecular solvent. It can thereby be questioned whether the effect of lowering T_g of the polymer host through inclusion of side chains represents any useful way toward improved ion transport, unless the side chains are also particularly designed to promote ion conduction paths.

It is interesting to note that the calculated diffusion coefficients—which are generally used to estimate conductivity in MD simulations of SPEs—do not clearly reflect the true nature of the ionic mobility in these simulated systems. This is likely due to slow dynamics in high-viscosity systems such as polymer electrolytes, which render it challenging to reach a completely diffusive regime even during extended simulation times (1 μs).
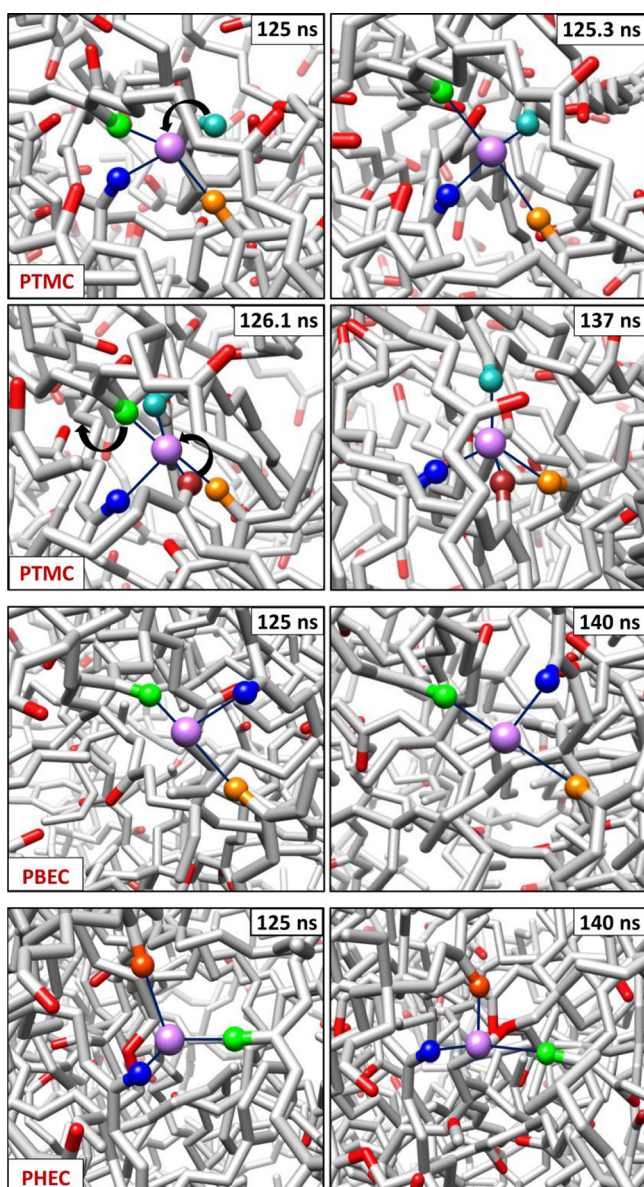
Figure 7. Schematic illustration of the Li$^+$ coordination sphere of individual ions in (a) PTMC at four different time frames during the trajectory and in (b) PBEC and (c) PHEC at two different time frames during the trajectory. The polymer chains are depicted by the gray color except the carbonyl oxygens (and the ethereal O of the side chain in PHEC), which are in red. Carbonyl oxygen atoms within 2.5 Å of the Li ion are shown with different colors (orange, light green, light blue, brown, and dark blue). Li$^+$ is presented in purple. H atoms and anions are omitted for better visualization.

ASSOCIATED CONTENT

ⓈⒾ Supporting Information

The Supporting Information is available free of charge at https://pubs.acs.org/doi/10.1021/acs.macromol.9b01912.

> Partial charges used, simulated T_g values, DSC traces, estimated ionic mobilities, ionic conductivities, MSD functions and slopes, calculated diffusion coefficients, RDFs for nonscaled charge models, and mathematical description of the analysis methods (PDF)

AUTHOR INFORMATION

Corresponding Author

Daniel Brandell − *Department of Chemistry − Ångström Laboratory, Uppsala University, SE-751 21 Uppsala, Sweden;* ⓞ orcid.org/0000-0002-8019-2801; Email: Daniel.Brandell@kemi.uu.se

Authors

Mahsa Ebadi − *Department of Chemistry − Ångström Laboratory, Uppsala University, SE-751 21 Uppsala, Sweden;* ⓞ orcid.org/0000-0001-8525-7339

Therese Eriksson − *Department of Chemistry − Ångström Laboratory, Uppsala University, SE-751 21 Uppsala, Sweden*

Prithwiraj Mandal − *Department of Chemistry − Ångström Laboratory, Uppsala University, SE-751 21 Uppsala, Sweden*

Luciano T. Costa − *Instituto de Quimica−Departamento de Fisico-quimica, Universidade Federal Fluminense, CEP 24020-150 Niterói, Brazil;* ⓞ orcid.org/0000-0002-9967-4034

C. Moyses Araujo − *Materials Theory Division, Department of Physics and Astronomy, Uppsala University, SE-751 20 Uppsala, Sweden;* ⓞ orcid.org/0000-0001-5192-0016

Jonas Mindemark − *Department of Chemistry − Ångström Laboratory, Uppsala University, SE-751 21 Uppsala, Sweden;* ⓞ orcid.org/0000-0002-9862-7375

Complete contact information is available at: https://pubs.acs.org/10.1021/acs.macromol.9b01912

Notes

The authors declare no competing financial interest.

REFERENCES

(1) Xu, W.; Wang, J.; Ding, F.; Chen, X.; Nasybulin, E.; Zhang, Y.; Zhang, J.-G. Lithium Metal Anodes for Rechargeable Batteries. *Energy Environ. Sci.* **2014**, *7*, 513−537.

(2) Ratner, M. A.; Shriver, D. F. Ion Transport in Solvent-Free Polymers. *Chem. Rev.* **1988**, *88*, 109−124.

(3) Ratner, M. A.; Johansson, P.; Shriver, D. F. Polymer Electrolytes: Ionic Transport Mechanisms and Relaxation Coupling. *MRS Bull.* **2000**, *25*, 31−37.

(4) Bresser, D.; Lyonnard, S.; Iojoiu, C.; Picard, L.; Passerini, S. Decoupling Segmental Relaxation and Ionic Conductivity for Lithium-Ion Polymer Electrolytes. *Mol. Syst. Des. Eng.* **2019**, *4*, 779−792.

(5) Wang, Y.; Fan, F.; Agapov, A. L.; Yu, X.; Hong, K.; Mays, J.; Sokolov, A. P. Design of Superionic Polymers—New Insights from Walden Plot Analysis. *Solid State Ionics* **2014**, *262*, 782−784.

(6) Angell, C. A. Polymer Electrolytes—Some Principles, Cautions, and New Practices. *Electrochim. Acta* **2017**, *250*, 368−375.

(7) Scrosati, B.; Garche, J. Lithium Batteries: Status, Prospects and Future. *J. Power Sources* **2010**, *195*, 2419−2430.

(8) Di Noto, V.; Lavina, S.; Giffin, G. A.; Negro, E.; Scrosati, B. Polymer Electrolytes: Present, Past and Future. *Electrochim. Acta* **2011**, *57*, 4.

(9) Xue, Z.; He, D.; Xie, X. Poly(Ethylene Oxide)-Based Electrolytes for Lithium-Ion Batteries. *J. Mater. Chem. A* **2015**, *3*, 19218−19253.

(10) Fenton, D. E.; Parker, J. M.; Wright, P. V. Complexes of Alkali Metal Ions with Poly(Ethylene Oxide). *Polymer* **1973**, *14*, 589.

(11) Wright, P. V. Electrical Conductivity in Ionic Complexes of Poly(Ethylene Oxide). *Br. Polym. J.* **1975**, *7*, 319.

(12) Armand, M. B.; Chabagno, J. M.; Duclot, M. Polymeric Solid Electrolytes. In *Second International Meeting on Solid Electrolytes*, 1978.

(13) Bannister, D.; Davies, G.; Ward, I.; McIntyre, J. Ionic Conductivities of Poly(Methoxy Polyethylene Glycol Monomethacrylate) Complexes with $LiSO_3CH_3$. *Polymer* **1984**, *25*, 1600−1602.

(14) Meyer, B. W. H. Polymer Electrolytes for Lithium-Ion Batteries. *Adv. Mater.* **1998**, *10*, 439−448.

(15) Barteau, K. P.; Wolffs, M.; Lynd, N. A.; Fredrickson, G. H.; Kramer, E. J.; Hawker, C. J. Allyl Glycidyl Ether-Based Polymer Electrolytes for Room Temperature Lithium Batteries. *Macromolecules* **2013**, *46*, 8988−8994.

(16) Mindemark, J.; Imholt, L.; Brandell, D. Synthesis of High Molecular Flexibility Polycarbonates for Solid Polymer Electrolytes. *Electrochim. Acta* **2015**, *175*, 247−253.

(17) Mindemark, J.; Imholt, L.; Montero, J.; Brandell, D. Allyl Ethers as Combined Plasticizing and Crosslinkable Side Groups in Polycarbonate-Based Polymer Electrolytes for Solid-State Li Batteries. *J. Polym. Sci., Part A: Polym. Chem.* **2016**, *54*, 2128−2135.

(18) Konieczynska, M. D.; Lin, X.; Zhang, H.; Grinstaff, M. W. Synthesis of Aliphatic Poly(Ether 1,2-Glycerol Carbonate)s via Copolymerization of CO_2 with Glycidyl Ethers Using a Cobalt Salen Catalyst and Study of a Thermally Stable Solid Polymer Electrolyte. *ACS Macro Lett.* **2015**, *4*, 533−537.

(19) Tominaga, Y.; Shimomura, T.; Nakamura, M. Alternating Copolymers of Carbon Dioxide with Glycidyl Ethers for Novel Ion-Conductive Polymer Electrolytes. *Polymer* **2010**, *51*, 4295−4298.

(20) Motogami, K.; Kono, M.; Mori, S.; Watanabe, M.; Ogata, N. A New Polymer Electrolyte Based on Polyglycidylether. *Electrochim. Acta* **1992**, *37*, 1725−1727.

(21) Nakamura, M.; Tominaga, Y. Utilization of Carbon Dioxide for Polymer Electrolytes [II]: Synthesis of Alternating Copolymers with Glycidyl Ethers as Novel Ion-Conductive Polymers. *Electrochim. Acta* **2011**, *57*, 36−39.

(22) Itoh, T.; Fujita, K.; Inoue, K.; Iwama, H.; Kondoh, K.; Uno, T.; Kubo, M. Solid Polymer Electrolytes Based on Alternating Copolymers of Vinyl Ethers with Methoxy Oligo(Ethyleneoxy)Ethyl Groups and Vinylene Carbonate. *Electrochim. Acta* **2013**, *112*, 221−229.

(23) Mindemark, J.; Lacey, M. J.; Bowden, T.; Brandell, D. Beyond PEO—Alternative Host Materials for Li + -Conducting Solid Polymer Electrolytes. *Prog. Polym. Sci.* **2018**, *81*, 114−143.

(24) Sun, B.; Mindemark, J.; Edström, K.; Brandell, D. Polycarbonate-Based Solid Polymer Electrolytes for Li-Ion Batteries. *Solid State Ionics* **2014**, *262*, 738−742.

(25) Mindemark, J.; Sun, B.; Törmä, E.; Brandell, D. High-Performance Solid Polymer Electrolytes for Lithium Batteries Operational at Ambient Temperature. *J. Power Sources* **2015**, *298*, 166−170.

(26) Silva, M. M.; Barros, S. C.; Smith, M. J.; MacCallum, J. R. Characterization of Solid Polymer Electrolytes Based on Poly-(Trimethylenecarbonate) and Lithium Tetrafluoroborate. *Electrochim. Acta* **2004**, *49*, 1887−1891.

(27) Silva, M. M.; Barbosa, P.; Evans, A.; Smith, M. J. Novel Solid Polymer Electrolytes Based on Poly(Trimethylene Carbonate) and Lithium Hexafluoroantimonate. *Solid State Sci.* **2006**, *8*, 1318−1321.

(28) Mindemark, J.; Sun, B.; Brandell, D. Hydroxyl-Functionalized Poly(Trimethylene Carbonate) Electrolytes for 3D-Electrode Configurations. *Polym. Chem.* **2015**, *6*, 4766−4774.

(29) Sun, B.; Asfaw, H. D.; Rehnlund, D.; Mindemark, J.; Nyholm, L.; Edström, K.; Brandell, D. Toward Solid-State 3D-Microbatteries Using Functionalized Polycarbonate-Based Polymer Electrolytes. *ACS Appl. Mater. Interfaces* **2018**, *10*, 2407−2413.

(30) Franco, A. A.; Rucci, A.; Brandell, D.; Frayret, C.; Gaberscek, M.; Jankowski, P.; Johansson, P. Boosting Rechargeable Batteries

R&D by Multiscale Modeling: Myth or Reality? *Chem. Rev.* **2019**, *119*, 4569−4627.

(31) Webb, M. A.; Jung, Y.; Pesko, D. M.; Savoie, B. M.; Yamamoto, U.; Coates, G. W.; Balsara, N. P.; Wang, Z.-G.; Miller, T. F. Systematic Computational and Experimental Investigation of Lithium-Ion Transport Mechanisms in Polyester-Based Polymer Electrolytes. *ACS Cent. Sci.* **2015**, *1*, 198−205.

(32) Pesko, D. M.; Webb, M. A.; Jung, Y.; Zheng, Q.; Miller, T. F.; Coates, G. W.; Balsara, N. P. Universal Relationship between Conductivity and Solvation-Site Connectivity in Ether-Based Polymer Electrolytes. *Macromolecules* **2016**, *49*, 5244−5255.

(33) Brooks, D. J.; Merinov, B. V.; Goddard, W. A.; Kozinsky, B.; Mailoa, J. Atomistic Description of Ionic Diffusion in PEO−LiTFSI: Effect of Temperature, Molecular Weight, and Ionic Concentration. *Macromolecules* **2018**, *51*, 8987−8995.

(34) Zheng, Q.; Pesko, D. M.; Savoie, B. M.; Timachova, K.; Hasan, A. L.; Smith, M. C.; Miller, T. F.; Coates, G. W.; Balsara, N. P. Optimizing Ion Transport in Polyether-Based Electrolytes for Lithium Batteries. *Macromolecules* **2018**, *51*, 2847−2858.

(35) Van Der Spoel, D.; Lindahl, E.; Hess, B.; Groenhof, G.; Mark, A. E.; Berendsen, H. J. C. GROMACS: Fast, Flexible, and Free. *J. Comput. Chem.* **2005**, *26*, 1701−1718.

(36) Abraham, M. J.; Murtola, T.; Schulz, R.; Pall, S.; Smith, J. C.; Hess, B.; Lindahl, E. Gromacs: High Performance Molecular Simulations through Multi-Level Parallelism from Laptops to Supercomputers. *SoftwareX* **2015**, *1−2*, 19−25.

(37) Martínez, L.; Andrade, R.; Birgin, E. G.; Martínez, J. M. PACKMOL: A Package for Building Initial Configurations for Molecular Dynamics Simulations. *J. Comput. Chem.* **2009**, *30*, 2157−2164.

(38) Jorgensen, W. L.; Maxwell, D. S.; Tirado-Rives, J. Development and Testing of the OPLS All-Atom Force Field on Conformational Energetics and Properties of Organic Liquids. *J. Am. Chem. Soc.* **1996**, *118*, 11225−11236.

(39) Lopes, J. N. C.; Padua, A. A. H. Molecular Force Field for Ionic Liquids Composed of Triflate or Bistriflylimide Anions. *J. Phys. Chem. B* **2004**, *108*, 16893−16898.

(40) *Maestro; MS Jaguar,Schrödinger*; Maestro, Schrödinger: New York, 2018.

(41) Shirts, M. R.; Klein, C.; Swails, J. M.; Yin, J.; Gilson, M. K.; Mobley, D. L.; Case, D. A.; Zhong, E. D. Lessons Learned from Comparing Molecular Dynamics Engines on the SAMPL5 Dataset. *J. Comput.-Aided Mol. Des.* **2017**, *31*, 147−161.

(42) Breneman, C. M.; Wiberg, K. B. Determining Atom-centered Monopoles from Molecular Electrostatic Potentials. The Need for High Sampling Density in Formamide Conformational Analysis. *J. Comput. Chem.* **1990**, *11*, 361−373.

(43) Frisch, M. J.; Trucks, G. W.; Schlegel, H. B.; Scuseria, G. E.; Robb, M. A.; Cheeseman, J. R.; Scalmani, G.; Barone, V.; Petersson, G. A.; Nakatsuji, H.; Li, X.; Caricato, M.; Marenich, A. V.; Bloino, J.; Janesko, B. G.; Gomperts, R.; Mennucci, B.; Hratch, D. J. *Gaussian 16*, Revision B.01; Gaussian, Inc.: Wallingford, CT, 2016.

(44) Becke, A. D. Density-functional Thermochemistry. III. The Role of Exact Exchange. *J. Chem. Phys.* **1993**, *98*, 5648−5652.

(45) Stephens, P. J.; Devlin, F. J.; Chabalowski, C. F.; Frisch, M. J. Ab Initio Calculation of Vibrational Absorption and Circular Dichroism Spectra Using Density Functional Force Fields. *J. Phys. Chem.* **1994**, *98*, 11623−11627.

(46) Kendall, R. A.; Dunning, T. H.; Harrison, R. J. Electron Affinities of the First-Row Atoms Revisited. Systematic Basis Sets and Wave Functions. *J. Chem. Phys.* **1992**, *96*, 6796−6806.

(47) Costa, L. T.; Sun, B.; Jeschull, F.; Brandell, D. Polymer-Ionic Liquid Ternary Systems for Li-Battery Electrolytes: Molecular Dynamics Studies of LiTFSI in a EMIm-TFSI and PEO Blend. *J. Chem. Phys.* **2015**, *143*, No. 024904.

(48) Chen, F.; Forsyth, M. Elucidation of Transport Mechanism and Enhanced Alkali Ion Transference Numbers in Mixed Alkali Metal−Organic Ionic Molten Salts. *Phys. Chem. Chem. Phys.* **2016**, *18*, 19336−19344.

(49) Chen, X.; Chen, F.; Liu, M. S.; Forsyth, M. Polymer Architecture Effect on Sodium Ion Transport in PSTFSI-Based Ionomers: A Molecular Dynamics Study. *Solid State Ionics* **2016**, *288*, 271−276.

(50) Buchholz, J.; Paul, W.; Varnik, F.; Binder, K. Cooling Rate Dependence of the Glass Transition Temperature of Polymer Melts: Molecular Dynamics Study. *J. Chem. Phys.* **2002**, *117*, 7364−7372.

(51) Pesko, D. M.; Jung, Y.; Hasan, A. L.; Webb, M. A.; Coates, G. W.; Miller, T. F.; Balsara, N. P. Effect of Monomer Structure on Ionic Conductivity in a Systematic Set of Polyester Electrolytes. *Solid State Ionics* **2016**, *289*, 118−124.

(52) Sun, B.; Mindemark, J.; Morozov, E. V.; Costa, L. T.; Bergman, M.; Johansson, P.; Fang, Y.; Furó, I.; Brandell, D. Ion Transport in Polycarbonate Based Solid Polymer Electrolytes: Experimental and Computational Investigations. *Phys. Chem. Chem. Phys.* **2016**, *18*, 9504−9513.

(53) Morioka, T.; Nakano, K.; Tominaga, Y. Ion-Conductive Properties of a Polymer Electrolyte Based on Ethylene Carbonate/ Ethylene Oxide Random Copolymer. *Macromol. Rapid Commun.* **2017**, *38*, 1600652.

(54) Molinari, N.; Mailoa, J. P.; Kozinsky, B. Effect of Salt Concentration on Ion Clustering and Transport in Polymer Solid Electrolytes: A Molecular Dynamics Study of PEO-LiTFSI. *Chem. Mater.* **2018**, *30*, 6298−6306.

(55) Costa, L. T.; Ribeiro, M. C. C. Molecular Dynamics Simulation of Polymer Electrolytes Based on Poly(Ethylene Oxide) and Ionic Liquids. II. Dynamical Properties. *J. Chem. Phys.* **2007**, *127*, 164901.

(56) Liu, H.; Maginn, E. Effect of Ion Structure on Conductivity in Lithium-Doped Ionic Liquid Electrolytes: A Molecular Dynamics Study. *J. Chem. Phys.* **2013**, *139*, 114508.

(57) Zhang, Y.; Maginn, E. J. Direct Correlation between Ionic Liquid Transport Properties and Ion Pair Lifetimes: A Molecular Dynamics Study. *J. Phys. Chem. Lett.* **2015**, *6*, 700−705.